Mon. Not. R. Astron. Soc. **000**, 1–15 (2008) Printed 21 January 2009 (MN LATEX style file v2.2)

On the width and shape of the corotation region for low-mass planets

S.-J. Paardekooper⋆ and J.C.B. Papaloizou
DAMTP, University of Cambridge, Wilberforce Road, Cambridge CB3 0WA, United Kingdom

arXiv:0901.2263v1 [astro-ph.EP] 15 Jan 2009

Draft version 21 January 2009

ABSTRACT

We study the coorbital flow for embedded, low mass planets. We provide a simple semi-analytic model for the corotation region, which is subsequently compared to high resolution numerical simulations. The model is used to derive an expression for the half-width of the horseshoe region, x_s, which in the limit of zero softening is given by $x_\mathrm{s}/r_\mathrm{p} = 1.68(q/h)^{1/2}$, where q is the planet to central star mass ratio, h is the disc aspect ratio and r_p the orbital radius. This is in very good agreement with the same quantity measured from simulations. This result is used to show that horseshoe drag is about an order of magnitude larger than the linear corotation torque in the zero softening limit. Thus the horseshoe drag, the sign of which depends on the gradient of specific vorticity, is important for estimates of the total torque acting on the planet. We further show that phenomena, such as the Lindblad wakes, with a radial separation from corotation of $\sim$ a pressure scale height H can affect x_s, even though for low-mass planets $x_\mathrm{s} \ll H$. The effect is to distort streamlines and to reduce x_s through the action of a back pressure. This effect is reduced for smaller gravitational softening parameters and planets of higher mass, for which x_s becomes comparable to H.

Key words: planetary systems: formation – planets and satellites: formation.

1 INTRODUCTION

Immediately after the discovery of the first extrasolar planet (Mayor & Queloz 1995), a Jupiter-mass planet in a very close orbit, it was realised that this class of planets, the Hot Jupiters, could not have been formed at their present location. In stead, they should have formed further out in the protoplanetary disc, and migrated inward afterwards. As outlined in Goldreich & Tremaine (1979, 1980), planets embedded in protoplanetary discs indeed will undergo orbital evolution through disc tides, and a great deal of theoretical work has been dedicated to understand the direction and magnitude of planetary migration (for an overview see Papaloizou et al. 2007).

One can distinguish three types of migration. High mass planets, comparable to Jupiter, open up deep gaps in their discs, after which they migrate on approximately a viscous time scale (Lin & Papaloizou 1986). This is called Type II migration (Ward 1997). Less massive planets, comparable to Saturn, embedded in massive discs may undergo fast Type III migration (Masset & Papaloizou 2003; Pepliński et al. 2008a). Both Type II and Type III migration may be directed inward or outward, depending on local conditions in the disc (Crida & Morbidelli 2007; Pepliński et al. 2008b), but the general trend is inward migration.

Low-mass planets, up to a few times the mass of the Earth ($\mathrm{M}_\oplus$), undergo Type I migration (Ward 1997). This type of migration is driven by a linear wave response in the disc, leading to a characteristic two-armed spiral pattern (Ogilvie & Lubow 2002). The waves can be understood to be excited at Lindblad resonances (Goldreich & Tremaine 1979) and lead to a torque on the planet that is due to asymmetries in the density, pressure and rotation profile in the disc (Ward 1997). The resulting migration direction is inward for all reasonable disc parameters (Korycansky & Pollack 1993; Tanaka et al. 2002).

Apart from this wave, or Lindblad, torque, embedded planets are also subject to corotation torques (Goldreich & Tremaine 1979). Two descriptions of the corotation torque exist in the literature. As advocated by Goldreich & Tremaine (1979), one can perform a linear analysis of the corotation resonance, which leads to a torque proportional to the radial gradient of specific vorticity, or vortensity, in the unperturbed disc. Semi-analytical and numerical studies lead to expressions for the total corotation torque (Korycansky & Pollack 1993; Tanaka et al. 2002) in two- and in three-dimensional discs. We will refer to this torque as the linear corotation torque.

A different view on the corotation torque was given by

⋆ E-mail: S.Paardekooper@damtp.cam.ac.uk

Ward (1991), who considered the torque due to material near the orbit of the planet that executes horseshoe turns. The total corotation torque is again proportional to the radial gradient of specific vorticity in the unperturbed disc, but the model contains a free parameter x_s, the width of the horseshoe region. We will refer to this torque as the horseshoe drag. The relation between the two descriptions has never been clarified so far.

Linear theory has been compared successfully against numerical hydrodynamical simulations, in 2D (D'Angelo et al. 2002; Nelson & Papaloizou 2004) as well as in 3D (D'Angelo et al. 2003). At this point we remark, however, that in these studies, only discs with small gradients in specific vorticity were considered, that is, cases where the corotation is supposed to be weak. For shallow surface density gradients, resulting in strong corotation torques, intermediate mass planets may reverse their direction of migration (Masset et al. 2006).

All studies mentioned so far have made use of the simplifying assumption that a barotropic (or isothermal) equation of state applies, in which case no energy equation needs to be solved. The dramatic effects of releasing this assumption were first noted in Paardekooper & Mellema (2006a), where it was shown that low-mass planets can migrate *outward* in non-isothermal discs. Subsequently it was realised that this was due to a radial entropy gradient in the unperturbed disc (Paardekooper & Mellema 2008), giving rise to a strong, positive corotation torque. Baruteau & Masset (2008) provided a linear analysis of the problem, and argued that a linear effect due to a background entropy gradient can be strong enough to reverse the torque on low-mass planets. However, Paardekooper & Papaloizou (2008) showed that this linear effect is in fact small, and that a non-linear effect is responsible for the torque reversal as seen in Paardekooper & Mellema (2006a).

The non-linear torque, as studied in Paardekooper & Papaloizou (2008), is closely related to the idea of horseshoe drag originally introduced by by Ward (1991) as both of these are produced by disc material undergoing horseshoe turns in the neighbourhood of the planet. For this reason it is very important to have a clear understanding of the horseshoe drag and in particular its relationship to linear corotation torques that are often used to estimate torques arising from coorbital effects. In this paper, we will provide an analysis of the horseshoe region for low-mass planets, in particular we determine its half-width x_s for softening lengths ranging between zero and the disc scale height. For simplicity we shall return to considering a barotropic equation of state and work with a two dimensional model. Since the horseshoe drag is proportional to x_s^4 (see Ward 1991), a good estimate of this parameter is critical in determining the total torque on the planet which is found in to be significantly larger than estimates based on linear theory for zero softening. In an accompanying paper, we perform a general study on the behaviour of the torques and their dependence on other parameters such as the disc viscosity.

The plan of this paper is as follows. In Section 2, we review the basic equations and introduce our local model. In Section 3, we study the structure of the corotation region, and in Section 4 we analyse the resulting streamlines. These are then compared with numerical hydrodynamic simulations in Section 5, after which we give a brief discussion and conclusions in Section 6.

2 BASIC EQUATIONS AND DISC MODELS

The basic equations are those of the conservation of mass, momentum and energy for a two dimensional disc in a frame rotating with angular velocity Ω_p. we adopt a cylindrical polar coordinate system (r,φ,z) with origin $(r=0)$ located at the central mass. The disc then occupies the plane $z=0$. The continuity equation and the equation of motion take the form

$$\frac{\partial\Sigma}{\partial t}=-\nabla\cdot(\Sigma\mathbf{v}) \tag{1}$$

and

$$\frac{D\mathbf{v}}{Dt}+2\Omega_\mathrm{p}\hat{\mathbf{k}}\times\mathbf{v}=-\frac{1}{\Sigma}\nabla\Pi-\nabla\Phi \tag{2}$$

respectively. Here, Σ denotes the surface density, $\mathbf{v}=(v_r,v_\varphi)$ the velocity, $\hat{\mathbf{k}}$ denotes the unit vector in the vertical direction, and Π the vertically integrated pressure. Thus

$$\Pi=\int_{-\infty}^{\infty}P dz. \tag{3}$$

The total potential Φ is taken to be $\Phi=\Phi_\mathrm{G}+\Omega_\mathrm{p}^2r^2/2$, where Φ_G is the gravitational potential. The convective derivative is defined by

$$\frac{D}{Dt}\equiv\frac{\partial}{\partial t}+\mathbf{v}\cdot\nabla. \tag{4}$$

We adopt a barotropic equation of state such that

$$\Pi=F(\Sigma), \tag{5}$$

with $F(\Sigma)$ being a prescribed function of Σ. The square of the sound speed is given by

$$c_\mathrm{s}^2=\frac{dF(\Sigma)}{d\Sigma}. \tag{6}$$

When a power law is adopted such that

$$F=K\Sigma^\beta, \tag{7}$$

with K and β being constants, $c_\mathrm{s}=\beta(\Pi/\Sigma)$. The discs we consider are assumed to be low mass with the Toomre parameter $Q=(\Omega c_\mathrm{s})/(\pi G\Sigma)\gg 1$. The self-gravity of the disc is accordingly neglected.

2.1 Global studies

The gravitational potential is assumed to be due to the central mass and perturbing planet such that $\Phi_\mathrm{G}=\Phi_\mathrm{G0}+\Phi_\mathrm{Gp}$, when the z dependence is neglected. These are given by

$$\Phi_\mathrm{G0}=\frac{-GM_*}{r}, \tag{8}$$

and

$$\Phi_\mathrm{Gp}=\frac{-GM_\mathrm{p}}{\sqrt{r^2+r_\mathrm{p}^2-2rr_\mathrm{p}\cos(\Delta\varphi)+b^2r_\mathrm{p}^2}}+\frac{GM_\mathrm{p}r\cos(\Delta\varphi)}{r_\mathrm{p}^2}, \tag{9}$$

where $\Delta\varphi=\varphi-\varphi_\mathrm{p}$. In the above M_* denotes the mass of the central object, with M_p, r_p, and φ_p denoting the mass,

orbital radius and angular coordinate of the protoplanet respectively. The gravitational softening parameter is b. The last term in (9) is the indirect term which accounts for the gravitational acceleration of the origin of coordinate system due to the action of the protoplanet.

Rather than neglecting the vertical dependence of the perturbing potential, one may adopt a vertical average based on the density, ρ, thus one replaces the expression (9) by its vertical average

$$\Phi_{\rm Gp} \rightarrow \frac{1}{\Sigma}\int_{-\infty}^{\infty}\rho\Phi_{\rm Gp}dz. \tag{10}$$

This procedure is more consistent with the view that the two dimensional disc representation should be derived from applying a vertical averaging procedure and accordingly provides a vertical average. On the other hand if vertical motions near the midplane are small, use of the unaveraged form may be appropriate for representing the structure there as in a stacked layer model (eg. Masset et al. 2006).

When $\Omega_{\rm p} = 0$ the reference frame is non rotating but non inertial as the origin accelerates together with the central mass due to the action of the protoplanet. Numerical calculations are most conveniently performed in a frame corotating with the protoplanet. Then $\Omega_{\rm p}$ becomes the circular Keplerian angular velocity at radius $r_{\rm p}$. At a general radius, r, the Keplerian angular velocity is given by $\Omega_{\rm K}(r) = (GM_*/r^3)^{1/2}$. Thus $\Omega_{\rm K}(r_{\rm p}) = \Omega_{\rm p}$. The local vertical scale height of the disc is then defined through $H = c_{\rm s}/\Omega_{\rm K}$. Hydrostatic equilibrium in the z direction implies that

$$\rho = \rho_0 \exp\left[-\int_0^z (z'/H^2)dz'\right], \tag{11}$$

where ρ_0 is the midplane density. The value of H at the disc midplane is a measure of the local disc semi-thickness. From now on H will be stand for this quantity.

2.2 Local Description

As we are interested in a local region close to the planet, it is useful to work with a form of the basic equations adapted for this purpose. We use the well known shearing box formalism (Ward 1991). This uses a Cartesian coordinate system (x, y, z) corotating with the protoplanet and with origin at the centre of the planet. The disc velocity in the unperturbed state with no protoplanet, is in the local approximation,$\mathbf{v} = (v_x, v_y, 0) = \mathbf{v}_0 = (0, -3\Omega_{\rm p}x/2, 0)$, corresponding to a linear shear. When a protoplanet is present the equation of motion may be written

$$\frac{\partial \mathbf{v}}{\partial t} + \mathbf{v}\cdot\nabla\mathbf{v} + 2\Omega_{\rm p}\hat{\mathbf{k}}\times\mathbf{v} = -\frac{1}{\Sigma}\nabla\Pi - \nabla\Phi_{\rm L}, \tag{12}$$

where $\Phi_{\rm L} = \Phi_{\rm Gp} - 3\Omega_{\rm p}^2x^2/2$. The protoplanet potential is here taken to be given by

$$\Phi_{\rm Gp} = \frac{-GM_{\rm p}}{\sqrt{x^2+y^2+b^2r_p^2}}. \tag{13}$$

The indirect term being small compared to the direct potential close to the planet is neglected. The continuity equation remains of the same form as equation (1).

3 THE COROTATION REGION

We now consider the structure of the corotation region. We begin by considering steady state solutions of the basic equations. In this case the two components of the equation (12) are

$$\mathbf{v}\cdot\nabla v_x - 2\Omega_{\rm p}v_y = -\frac{\partial(w+\Phi_{\rm L})}{\partial x}, \tag{14}$$

and

$$\mathbf{v}\cdot\nabla v_y + 2\Omega_{\rm p}v_x = -\frac{\partial(w+\Phi_{\rm L})}{\partial y}, \tag{15}$$

where we have introduced the enthalpy, $w(\Sigma)$, which is defined through $dw/d\Sigma = c_{\rm s}^2/\Sigma$ together with the specification that $w(0) = 0$.

3.1 A simple one dimensional model

We now simplify the problem by in the first instance neglecting the degree of freedom corresponding to epicyclic motions. These are not expected to play a major role in the horseshoe region. One expects a balance between the Coriolis force and potential gradient with $\mathbf{v}\cdot\nabla v_x$ being negligible in equation (14). Neglecting this term is precisely the approximation often used in celestial mechanics to enable the derivation of a second order differential equation describing particle motion on horseshoe orbits. It breaks down only close to the protoplanet. In the next subsection, we discuss a more complete description of the coorbital region.

Adopting this approximation and using equation (14) we set

$$v_y = \frac{1}{2\Omega_{\rm p}}\frac{\partial\chi}{\partial x} = -\frac{1}{\Sigma}\frac{\partial\psi}{\partial x}, \tag{16}$$

where $\chi = w + \Phi_{\rm L}$, with ψ being the stream function. Equations (14) and (15) may also be written in the form

$$\left(2\Omega_{\rm p} + \frac{\partial v_y}{\partial x}\right)\hat{\mathbf{k}}\times\mathbf{v} = -\nabla\left(\frac{1}{2}v_y^2 + w + \Phi_{\rm L}\right). \tag{17}$$

From this and the steady state form of the continuity equation (1) it follows that both

$$E_0(\psi) = \left(\frac{1}{2}v_y^2 + w + \Phi_{\rm L}\right) \quad \text{and} \quad \xi_0(\psi) = \frac{\left(2\Omega_{\rm p} + \frac{\partial v_y}{\partial x}\right)}{\Sigma}$$

are constant on streamlines. These are statements of the conservation of the Bernoulli constant and the specific vorticity or vortensity on streamlines under the approximation used here which has the consequence that the contribution from the radial velocity is neglected. We note that the functional forms of $E_0(\psi)$ and $\xi_0(\psi)$ cannot be determined from the inviscid equations but have to be prescribed externally. From (16) it then follows that

$$\frac{1}{2\Omega_{\rm p}}\frac{\partial^2\chi}{\partial x^2} + 2\Omega_{\rm p} = \xi_0\Sigma. \tag{18}$$

Using the fact that $w(\Sigma) = \chi - \Phi_{\rm L}$ to eliminate Σ, a single equation for χ then results. We note that when a power law equation of state is used with $\beta = 2$, see (7), $w(\Sigma) = 2K\Sigma$, and we have the very simple relation

$$c_s^2 = \chi - \Phi_{\rm L}. \tag{19}$$

We thus obtain an equation for χ of the form

$$\frac{1}{2\Omega_{\rm p}}\frac{\partial^2\chi}{\partial x^2}+2\Omega_{\rm p}=\frac{\xi_0\Sigma}{c_{\rm s}^2}(\chi-\Phi_{\rm L}). \tag{20}$$

Setting $\chi = Y - 3\Omega_{\rm p}^2x^2/2$, this leads to

$$Y=\Phi_{\rm Gp}+\frac{c_{\rm s}^2}{2\xi_0\Sigma\Omega_{\rm p}}\frac{\partial^2 Y}{\partial x^2}+\frac{c_{\rm s}^2\Omega_{\rm p}}{2\xi_0\Sigma}. \tag{21}$$

We comment that although we adopted a power law equation of state with $\beta = 2$ to obtain (21), because w is a linear function of Σ in this case, the same equation applies to any barotropic equation of state in the regime where the surface density variations are small enough that only first order variations in the equation of state need to be considered. Then $c_{\rm s}^2/\Sigma$ is taken to be the constant background value. Of course when $\beta = 2$, $c_{\rm s}^2/\Sigma = 2K =$ constant regardless.

3.1.1 Solution for the coorbital region

Equation (21) contains no y derivatives and can accordingly be solved as a second order differential equation. Adopting the boundary condition that Y is bounded for $|x| \to \infty$ the solution can be written down in the standard form

$$Y=-\int_{-\infty}^{\infty}G(x,x')\left(\Omega_{\rm p}^2+\Phi_{\rm Gp}(x',y)\left(\frac{2\xi_0\Sigma\Omega_{\rm p}}{c_{\rm s}^2}\right)\right)dx', \tag{22}$$

where unless explicitly stated, quantities in this and other integrands are evaluated at (x', y') and the Green's function satisfies

$$\frac{\partial^2 G(x,x')}{\partial x'^2}-G(x,x')\left(\frac{2\xi_0\Sigma\Omega_{\rm p}}{c_{\rm s}^2}\right)_{x=x'}=\delta(x-x'). \tag{23}$$

with $G(x, x') \to 0$ for $|x'| \to \infty$. Having found $Y = \chi + 3\Omega_{\rm p}^2x^2/2$, the streamlines can be found from

$$E_0(\psi)=\frac{1}{8\Omega_{\rm p}^2}\left(\frac{\partial\chi}{\partial x}\right)^2+\chi \tag{24}$$

which is constant on them.

3.1.2 Constant vortensity

The corotation region is generally of small radial extent so that the quantity ξ_0, representing the variation of vortensity should be approximately constant unless the profile is very sharp. Therefore for reasonable smoothly varying cases vortensity variation is not expected to have much effect on the the coorbital structure except possibly for large softening cases perturbed by the density wakes associated with Lindblad torques (see below). Accordingly we shall specialise to the case of constant vortensity while retaining $\beta = 2$, so that both $\Sigma/c_{\rm s}^2$ and ξ_0 are constant. By considering large distances from the protoplanet, we infer that $\xi_0 = \Omega_{\rm p}/(2\Sigma_0)$, where Σ_0 is the uniform surface density at large distances from the protoplanet. Determination of the Green's function is straightforward in this case. We obtain

$$G(x,x')=-\frac{1}{2|k|}\exp\left(-|k||x-x'|\right), \tag{25}$$

where

$$k^2=\frac{\Omega_{\rm p}^2}{c_{\rm s0}^2}\equiv H^{-2}, \tag{26}$$

where $c_{\rm s0}$ is the uniform sound speed at large distances from the protoplanet and H is the scale height.

Although solution of (21) is straightforward, we comment that the scale of the decay of the Green's function is the scale height and thus phenomena that distance away from the protoplanet and not included here, such as the prominent wakes associated with Lindblad torques, can distort the flow (see below). In principle this effect could be included through the boundary conditions on G but we shall not consider it further in this section.

3.1.3 Asymptotic series and softened gravity model

We note also that in this limit, provided ξ_0 also varies on a length scale significantly exceeding, H, one can find a solution of equation (21) in the form of an asymptotic series in ascending powers of $c_{\rm s}^2$ or equivalently $H^2/|y|^2$. The zero order solution being simply $Y = \Phi_{\rm Gp} + \frac{c_{\rm s}^2\Omega_{\rm p}}{2\xi_0\Sigma}$, and we note here that the second term is a constant if ξ_0 is constant and may be discarded, or equivalently $\chi = \Phi_{\rm L}$. The streamlines are then found from (24) using this value of χ. We comment that this result would be obtained if pressure was neglected completely. Thus we describe it as the softened gravity limit and it should apply to streamlines at a distance greater than $\sim H$ from the protoplanet. It can also be obtained when the approximation of neglecting the acceleration in the x direction is not made at the outset. We now consider a modification of the above model that enables a more realistic treatment of regions close to the planet. However, this makes it two dimensional and accordingly more complex.

3.2 Modification close to the planet

We begin by noting that the system may be regarded as being governed by the components of the equation of motion (14) and (15) together with a complete statement of the conservation of vortensity in the form

$$\xi_0(\psi)\Sigma=\left(2\Omega_{\rm p}+\frac{\partial v_y}{\partial x}-\frac{\partial v_x}{\partial y}\right) \tag{27}$$

This equation should be regarded as replacing the continuity equation in those governing the model. The simple one dimensional model is obtained by using only (14) and (27) with v_x being neglected. Equation (15) is then used as an auxiliary equation to subsequently determine v_x. We now retain v_x in equation (27) which now needs to be specified using equation (15) in advance. We shall retain the approximation of neglecting v_x or equivalently the radial acceleration equation in (15). Thus as before we have

$$v_y=\frac{1}{2\Omega_{\rm p}}\frac{\partial\chi}{\partial x}. \tag{28}$$

Equation(14) gives

$$v_x\left(2\Omega_{\rm p}+\frac{\partial v_y}{\partial x}\right)=-\frac{\partial(\chi+v_y^2/2)}{\partial y}. \tag{29}$$

We make the approximation of replacing v_y in this equation by the unperturbed Keplerian value $v_y = -3x\Omega_{\rm p}/2$.This leads to

$$v_x=-\frac{2}{\Omega_{\rm p}}\frac{\partial\chi}{\partial y}. \tag{30}$$

We comment that we have found the above equation to be satisfied close to the planet in numerical simulations (see below).
Using (28), (30) and again adopting a power law equation of state with $\beta = 2$ and using (19), equation (27) leads to

$$\mathcal{D}^2 Y = \frac{2\Omega_{\rm p}\xi_0\Sigma}{c_{\rm s}^2}(Y - \Phi_{\rm Gp}) - \Omega_{\rm p}^2, \quad (31)$$

where the operator

$$\mathcal{D}^2 \equiv \frac{\partial}{\partial x^2} + 4\frac{\partial}{\partial y^2} \quad (32)$$

and we recall $Y = \chi + 3\Omega_{\rm p}^2 x^2/2$. The required solution of equation (31) can be written as

$$Y = -\int_{-\infty}^{\infty} G(x, y, x', y') \left(\Omega_{\rm p}^2 + \left(\frac{2\xi_0\Sigma\Omega_{\rm p}}{c_{\rm s}^2}\right)\Phi_{\rm Gp}\right) dx'dy', \quad (33)$$

where $G(x, y, x', y')$ is a two dimensional Green's function. When the vortensity is constant, and the Green's function that vanishes at ∞, it is given by

$$G(x, y, x', y') = -\frac{1}{4\pi}K_0(k\sqrt{(x - x')^2 + (y - y')^2/4}), \quad (34)$$

where as in standard notation K_0 is the Bessel function (this is readily obtained after scaling the y coordinate to transform $\mathcal{D}^2$ into the Laplacian). When comparing with the corresponding result obtained from the one dimensional treatment given by equation (22), we see that there is a two dimensional as compared to a one dimensional integration. The additional integration over y' acts like a smoothing on a length scale H.

The streamlines are in general determined from the Bernoulli condition that $(\mathbf{v}^2/2 + w + \Phi_{\rm L})$ be constant on them. This reduces to the condition given through equation (24) under the approximation scheme used to derive (31). We further remark that the scale of the flow in the y direction then becomes larger than H so we may perform the integration over y' keeping other quantities fixed. Using the result that

$$\frac{1}{2}\int_{-\infty}^{\infty} K_0(k\sqrt{(x - x')^2 + (y - y')^2/4})dy' = \frac{\pi}{|k|}\exp(-|k(x - x')|), \quad (35)$$

we then recover equation (22) for the simple one dimensional model.

We may also develop an asymptotic sequence as in section 3.1.3 starting with $Y = \Phi_{\rm Gp} - \Omega_{\rm p}^2 + c_{\rm s}^2\Omega_{\rm p}/(2\xi_0\Sigma)$, with the last two terms being constant, and then iterating (31) to find successive corrections to Y. Thus use of the two dimensional model imparts a smoothing in the y direction, with a length scale H, to the one dimensional model. This causes differences close to the planet for small softening.

4 STREAMLINE CALCULATIONS

We have used the simple one dimensional model to obtain χ and determine streamlines for the constant vortensity case using a range of softening lengths. We perform the integral specified in equation (22) in conjunction with equation (24). For comparison purposes we also obtained streamlines using equation (33), instead of (22). In this case the Green's function and integration are of course two dimensional.

4.1 Dimensionless scalings

Adopting H evaluated at the origin for the unperturbed flow as the unit of length, it is straightforward to see that apart from ξ_0, the distribution of specific vorticity, if b/h is fixed, the streamlines are characterised by only one parameter, q/h^3, where q is ratio of the mass of the protoplanet to the mass of central star and $h = H/r_{\rm p}$ is the disc aspect ratio (see e.g. Korycansky & Papaloizou 1996). We work with the power law equation of state with $\beta = 2$. In that case $c_{\rm s}^2/\Sigma$ is constant. In the local model, the adoption of a linear shear means that the background vorticity is a constant $= (1/2)\Omega_{\rm p}$. Therefore for constant vortensity the background surface density is a constant $= \Sigma_0$ and $\xi_0 = \Omega_{\rm p}/(2\Sigma_0)$. The units are arbitrary and so we choose these such that $\Sigma = 1$ at the origin in the unperturbed flow.

Streamlines for constant vortensity obtained for the simple one dimensional model from (22) with $q/h^3 = 0.0252$ and $b/h = 0.6$ are shown in Fig. 1. This parameterization corresponds to 1 $M_\oplus$ in a disc with $H/r_{\rm p} \sim 0.05$. The streamlines fall naturally into two groups, the first coming from $y > 0$ and $x > 0$ and the second coming from $y < 0$ and $x < 0$. For each of these classes a subset passes by the planet while the remainder undergoes a horseshoe turn. Those undergoing horseshoe turns constitute the horseshoe region, which is separated from the remaining domain by two separatrices. For the constant vortensity case, the flow has both left-right and up-down symmetry implying an X point at the centre of the protoplanet. When the vortensity is not constant this symmetry is in general lost.

The streamlines shown in the upper left panel of Fig. 1 corresponding to $q/h^3 = 0.0252$ and $b/h = 0.6$. have a horseshoe width of $\sim 0.25H$. To illustrate the dependence on q we also show the streamlines for $q/h^3 = 0.0126$ and $b/h = 0.6$. These suggest that the horseshoe width is proportional to $q^{1/2}$. This result can also be derived by considering the streamline at the centre of the protoplanet. At this location, where $x = \partial\chi/\partial x = 0$, equation (33) gives

$$\chi = Y = -\frac{1}{H^2}\int_{-\infty}^{\infty} G(0, 0, x', y')\Phi_{\rm Gp}dx'dy' + c_{\rm s}^2\Omega_{\rm p}/(2\xi_0\Sigma), \quad (36)$$

there being a corresponding expression derived from equation (22). The horseshoe width, $x_{\rm s}$, is obtained by equating this expression to $c_{\rm s}^2\Omega_{\rm p}/(2\xi_0\Sigma) - 3\Omega_{\rm p}^2 x_{\rm s}^2/8$, being the value of $E_0(\psi)$ obtained from (24) at large distances. Hence very generally,

$$x_{\rm s} \propto \sqrt{|\Phi_{\rm Gp}|} \propto \sqrt{q}. \quad (37)$$

To be more precise, performing the integral (36) for the two dimensional case we find that

$$\frac{x_{\rm s}^2}{r_{\rm p}^2} = \frac{4q}{3\pi h}\int_0^{\infty}\int_0^{2\pi} \frac{K_0(r)r}{\sqrt{r^2(1 + 3\sin^2\theta) + b^2/h^2}}d\theta dr, \quad (38)$$

which can be simplified to

$$\frac{x_{\rm s}^2}{r_{\rm p}^2} = \frac{16q}{3\pi h}\int_0^{\infty} \frac{K_0(r)r}{\sqrt{4r^2 + b^2/h^2}}E\left(\sqrt{\frac{3r^2}{4r^2 + b^2/h^2}}\right)dr, \quad (39)$$

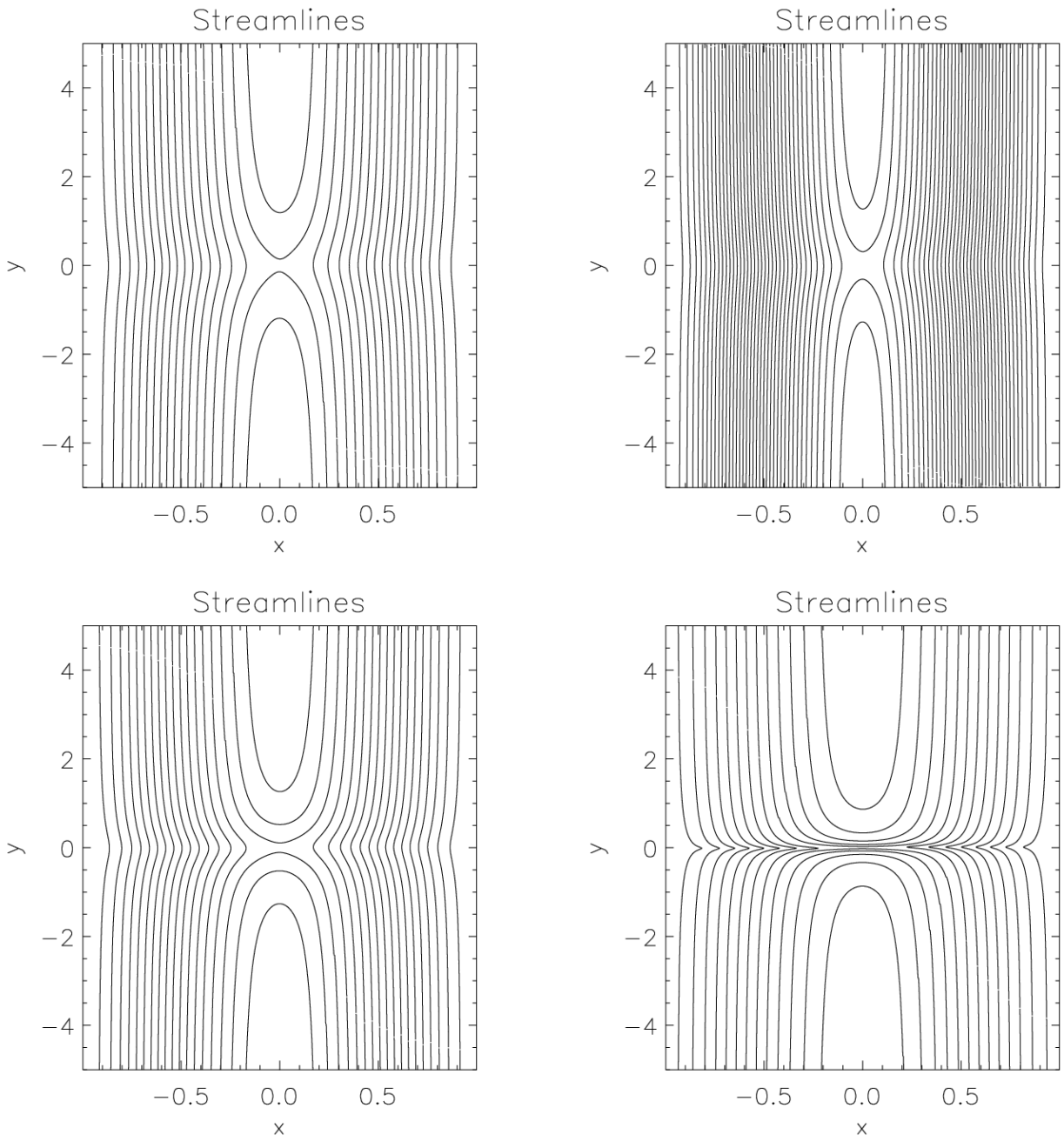

Figure 1. Streamlines for constant vortensity obtained using the simple one dimensional model. The plots are for $q/h^3 = 0.0252$ and $b/h = 0.6$ upper left panel, $q/h^3 = 0.0126$ and $b/h = 0.6$, upper right panel, $q/h^3 = 0.0252$ and $b/h = 0.3$, lower left panel and $q/h^3 = 0.0252$ and $b/h = 0.0252$, corresponding to the softening parameter being equal to the Bondi radius, lower right panel. For this and other similar figures the unit of length is the disc scale height, H, evaluated at the origin of the unperturbed flow.

where E denotes the complete elliptic integral of the first kind. For $b = 0$, this gives

$$x_{\rm s}|_{b=0} = \sqrt{\frac{4q}{3h}E\left(\frac{\sqrt{3}}{2}\right)}r_{\rm p} \approx 1.68\sqrt{\frac{q}{h}}\,r_{\rm p}, \tag{40}$$

which gives the horseshoe width in the limit of zero softening for the two dimensional model. We also note that in the limit $b \gg h$,

$$x_{\rm s} \sim \sqrt{\frac{8q}{3b}}r_{\rm p}, \tag{41}$$

which is the same result that would be obtained by neglecting pressure effects altogether.

To investigate the dependence on the softening parameter, we plot streamlines for the cases $q/h^3 = 0.0252$, with $b/h = 0.3$ and also with $b/h = 0.0252$ in Fig. 1. The second

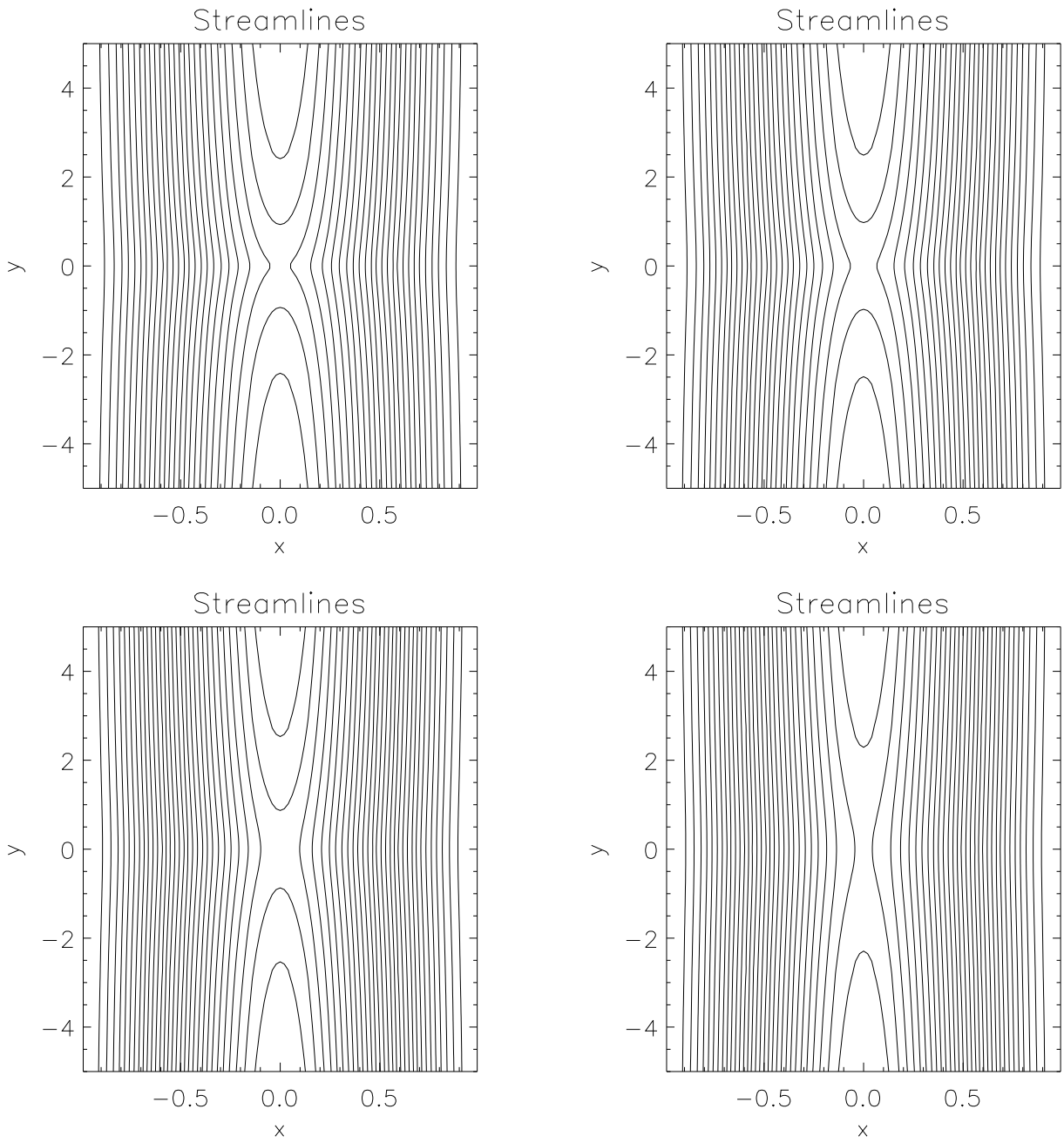

Figure 2. Streamlines for constant vortensity found using the two dimensional Green's function. The plots are for $q/h^3 = 0.0252$ and $b/h = 0.0252$, corresponding to the softening parameter being equal to the Bondi radius, upper left panel, and $q/h^3 = 0.0252$ with $b/h = 0.1$, upper right panel. In the lower left panel, $q/h^3 = 0.0252$ with $b/h = 0.3$, and in the lower right panel $q/h^3 = 0.0252$ with $b/h = 0.6$. The horseshoe region is wider for smaller softening lengths and converges to a well defined structure for $b \to 0$.

case corresponds to the softening parameter being equal to the Bondi radius $c_{\rm s}^2/(GM_{\rm p})$ for 1 $M_\oplus$ and a disc aspect ratio of $H/r_{\rm p} = 0.05$. Interior to the Bondi radius the gravity of the planet dominates and we expect a hydrostatic structure that does not participate in the horseshoe dynamics. We here remark that equation (22) obtained for the simple one dimensional model diverges logarithmically for $b \to 0$, but (33) is convergent.

In general as expected from (37) the horseshoe width increases as b decreases and the streamlines become more compressed and nearly horizontal near $y = 0$ indicating that the acceleration in the radial direction should not be neglected for small softening as has been done in the simple one dimensional model. In spite of this, the behaviour of the streamlines for $y > H$ is very similar for fixed q and the different values of b in these cases. This is in line with the existence of the asymptotic solution discussed above.

Streamlines for constant vortensity when the two di-

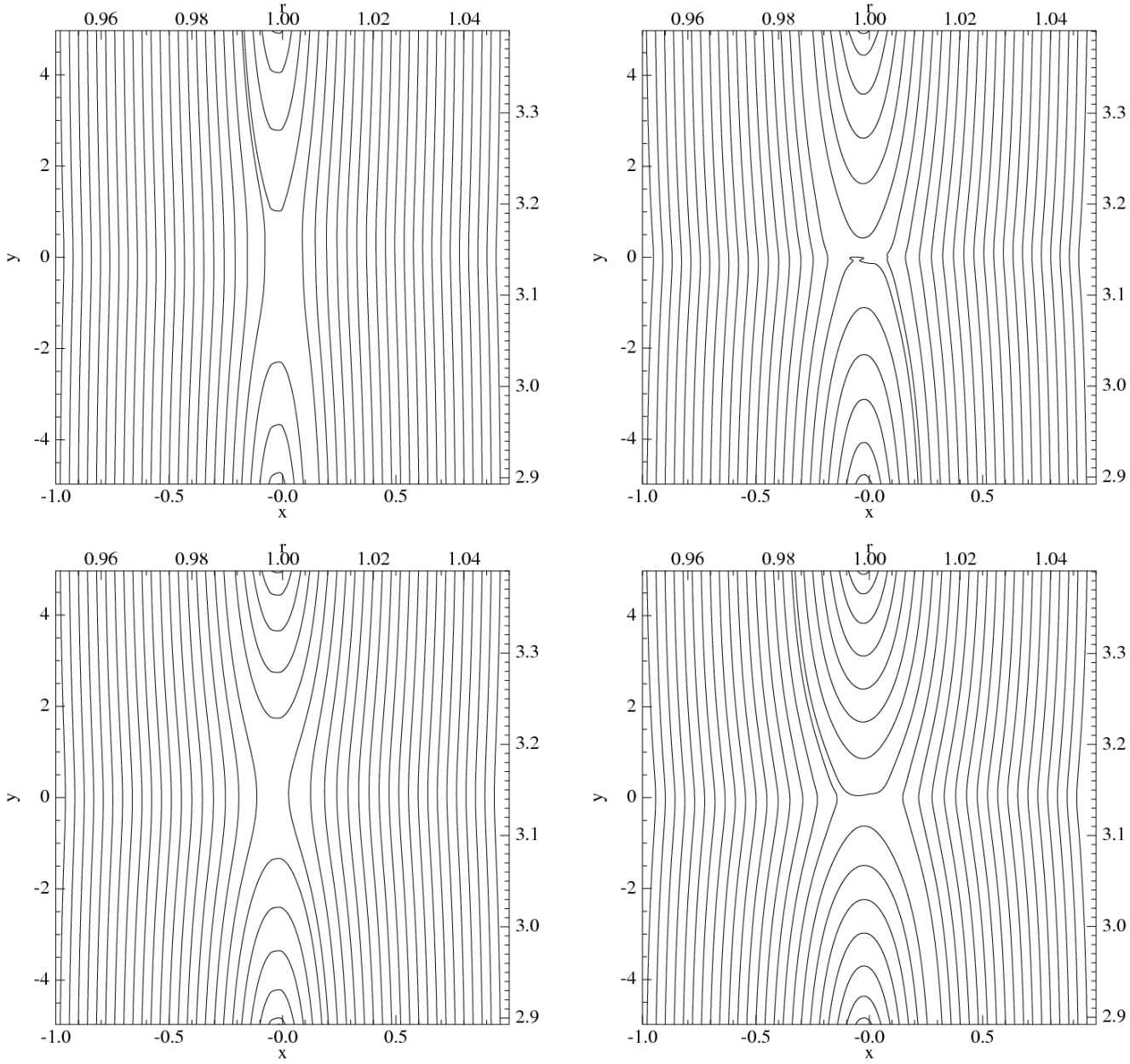

Figure 3. Streamlines, obtained from hydrodynamical simulations for constant vortensity and $q/h^3 = 0.0252$. Left panels: $b/h = 0.6$, right panels: $b/h = 0.025$. Top panels: full potential without cut off, bottom panels: the cut off procedure was adopted.

mensional Green's function is used are given in Fig. 2. These are for $q/h^3 = 0.0252$ with $b/h = 0.0252$, corresponding to the softening parameter being equal to the Bondi radius, together with plots obtained for $b/h = 0.1$, $b/h = 0.3$ and $b/h = 0.6$. Use of the two dimensional Green's function smooths the potential and makes the horseshoe region narrower compared to the simple one dimensional case. When $b = 0.6h$, the horseshoe width was $0.21H$ being about 20% smaller than that found using the simple one dimensional model. However, the horseshoe width converges in the limit of zero softening being about 30% wider than when $b/h = 0.6$.

We remark that using a potential vertically averaged with weight ρ, equivalent to a vertical smoothing, but retaining the formalism leading to equation(22) has a similar effect to using the two dimensional Green's function including convergence for $b \to 0$.

The discussion presented above was for low-mass planets, for which the Bondi radius is smaller than the radius of its Hill sphere $r_p(q/3)^{1/3}$. This condition is equivalent to the requirement that $q < h^3/\sqrt{3}$. In this regime we found no circulating streamlines close to the planet when the vortensity is constant. For more massive planets with $q > h^3/\sqrt{3}$, a circulating region is expected to interior to the Hill sphere. This limit was recently considered analytically in Pepliński (2008). We show an example of the resulting streamlines ob-

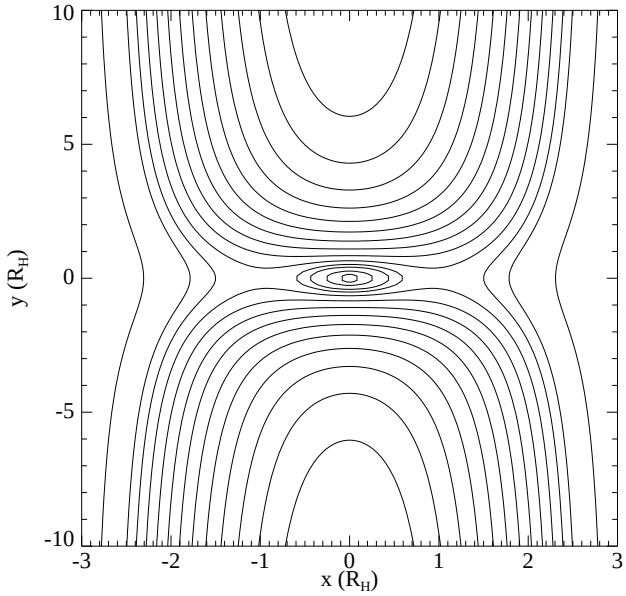

Figure 4. Streamlines close to the planet in the limit $q \gg h^3/\sqrt{3}$, in which case a circulating region within the Hill sphere arises. The unit of distance in this figure is Hill radius $R_H = (q/3)^{1/3} r_{\rm p}$.

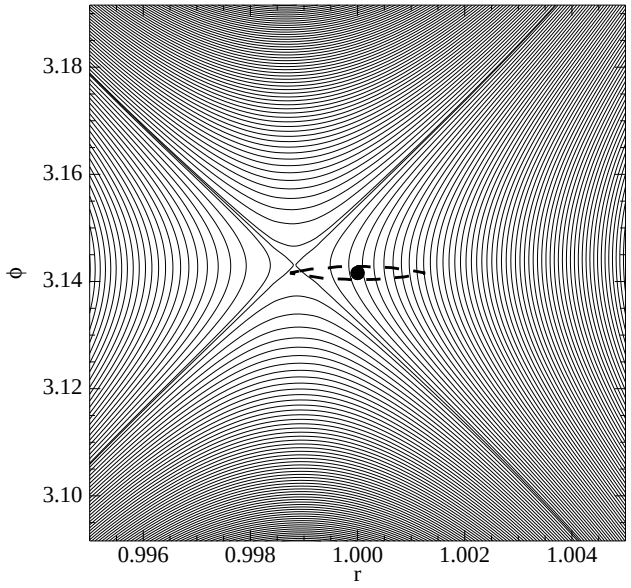

Figure 5. Streamlines close to the planet for $q/h^3 = 0.0252$ and $b/h = 0.6$ for a disc with constant vortensity. The planet is indicated by the filled circle, and the dashed contour indicates the Bondi radius. The cut off procedure was adopted for this simulation.

tained from our model in this limit in Fig. 4. Even though important non linear effects such as the onset of gap formation are not included (Papaloizou et al. 2007) there is indeed a circulating region within the Hill sphere in this case.

However such closed streamlines might in general be expected significantly interior to the Bondi radius for matter bound to a low mass planet. We comment that this issue is sensitive to model details such as the specification of the vortensity profile. To illustrate this, consider the situation when this bound matter appears almost stationary in the rotating frame such that circulating streamlines would be expected. This matter would have to have significantly lower vortensity than its surroundings. To see this we note that for a staionary solution $\chi = 0$, and $Y = 3\Omega_p^2 x^2/2$. With this specification, equation (31) gives

$$\frac{2\Omega_{\rm p} c_{\rm s}^2}{\xi_0 \Sigma} = \frac{3\Omega_{\rm p}^2 x^2}{2} - \Phi_{\rm Gp}, \tag{42}$$

setting the vortensity profile to be such that $\xi_0 = 2\Omega_{\rm p}/\Sigma$, we obtain

$$c_{\rm s}^2 = \frac{3\Omega_{\rm p}^2 x^2}{2} - \Phi_{\rm Gp}, \tag{43}$$

which is the expected condition for hydrostatic equilibrium of the protoplanet under centrifugal and tidal forces for our baratropic equation of state. Note that to achieve this, the surface density should rapidly increase and hence the prescribed vortensity should correspondingly decrease towards the center of the protoplanet. On account of the attainment of a limiting form of the horseshoe region once the softening lenght b is smaller than the Bondi radius, we do not expect the details of behaviour at interior radii to significantly affect the results.

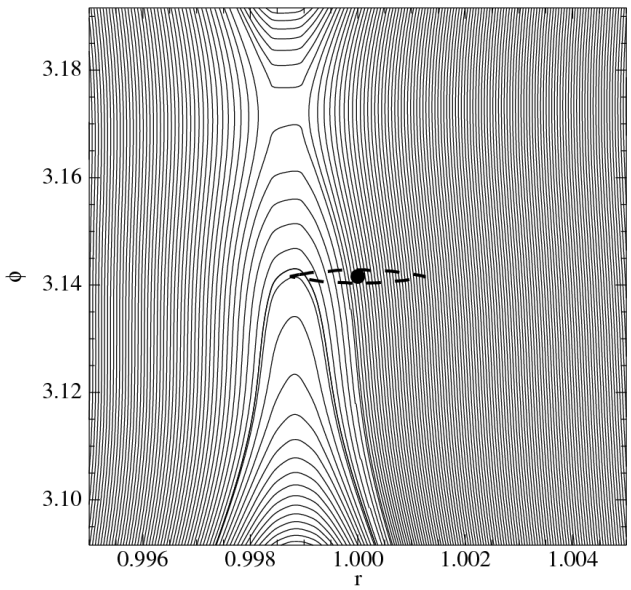

Figure 6. Streamlines close to the planet for $q/h^3 = 0.0252$ and $b/h = 0.6$ for a disc with constant vortensity. The planet is indicated by the filled circle, and the dashed contour indicates the Bondi radius. The full planet potential was adopted with no cut off.

5 NUMERICAL SIMULATIONS

In this section, we compare the streamline calculations of Section 4 with fully non linear hydrodynamical simulations.

5.1 Set up

We use the RODEO method (Paardekooper & Mellema 2006b) in two spatial dimensions, on a regular grid which when at its most extended, runs from $r = 0.5r_{\rm p}$ to $r = 1.8r_{\rm p}$ and which covers the whole 2π in azimuth. Since we want to resolve the horseshoe region for even the smallest planets we consider, a relatively high resolution is used. For the most extended grid this has 1024 cells in the radial and 4096 cells in the azimuthal direction. Then the resolution at the location of the planet is approximately $0.0015r_{\rm p}$ in both directions. Tests have shown that this resolution is sufficient to capture the horseshoe dynamics for $x_{\rm s} > 0.004r_{\rm p}$. We always ensure that we resolve the softening length $br_{\rm p}$ by at least 3 grid cells, which means that for the smallest values of b we consider an even higher resolution is was adopted. We take the disc to be inviscid and isothermal with uniform specific vorticity such that $\Sigma \propto r^{-3/2}$ for the unperturbed initial state.

We consider two kinds of simulation, the first adopted the perturbing potential given by equation (9) and adopted the most extended domain. The second type of simulation considers only the coorbital region extending from $r_{\rm p}-2H/3$ to $r_{\rm p}+2H/3$ and occupying the full 2π in azimuth. Non reflecting boundary conditions are applied at the radial boundaries such that material is allowed to leave and enter freely. We refer to this second type of simulation as having employed a cut off procedure. Results obtained with this type of simulation were checked with simulations employing the most extended domain but modifying the protoplanet perturbing potential such that it is given by equation (9) for $|r-r_{\rm p}| < 2H/3$, and zero otherwise. These gave very similar results. The cut-offs applied in these simulations exclude the bulk of the contributions from the Lindblad torques to the flow. Since either the planet potential vanishes in the region where they are normally generated or that region falls outside the computational domain. As remarked in Section 3, features on the order of one scale height away, such as phenomena associated with Lindblad torques, may affect the coorbital region even when this is much narrower than H. Differences between the results obtained from the two kinds of simulation we performed are consistent with this supposition.

5.2 Streamline analysis

We start by comparing the flow on a scale of H to that found using the model of Section 3 in Fig. 3, for two different values of the softening parameter b and the two types of simulation. To obtain $q/h^3 = 0.0252$ we set up 1 $\rm M_\oplus$ around a Solar mass star in a disc with $h = 0.05$. We compare the results illustrated in this figure with the corresponding results obtained using the two dimensional Green's function shown in Fig. 2. For the case of large softening, $b/h = 0.6$, without a cut off, although the streamline pattern appears similar, the width of the horseshoe region is about 22% smaller than that depicted in Fig. 2. When the cut off procedure is applied, the horseshoe region increases in width by about 50% (see below). This indicates that phenomena located in the region where the Lindblad torques are generated may play a significant role in shaping the coorbital region.

For smaller softening such that $b/h = 0.025$, corresponding to the softening parameter being equal to the Bondi radius, the differences between the two types of simulation is less extreme. The measured increase in $x_{\rm s}$ obtained on applying the cut off procedure amounts to 20%. In this case there is very good agreement between the simulation without a cut off and the model of Section 3 with the two dimensional Green's function illustrated in Fig. 2, with the values of $x_{\rm s}$ differing by several percent.

The dependence on softening can be understood as follows: the strength of phenomena related to Lindblad torques is determined by the planet potential at approximately a distance H from the planet, while the width of the horseshoe region depends on $|\Phi_{\rm Gp}|$ at the location of the planet. For a softening parameter comparable to h, the planet potential at these two locations is comparable. Therefore, it is relatively easy for Lindblad torque related phenomena to affect the coorbital region. For smaller softening, $|\Phi_{\rm Gp}|$ at the location of the planet increases, while the value at a distance H remains largely unchanged. For $b \ll h$, we expect the effect of phenomena originating a distance $\sim H$ from the planet to be smaller, and therefore there should be better agreement between the numerical simulations and the model of Section 3.

The effect of introducing the cut off is to produce larger corotational speeds directed towards the planet. These are eventually slowed down as the pressure gradient reduces, producing a stagnation point at, or very close to the planet's location. The faster moving material can originate further from the planet and so is associated with an increased horseshoe width.

The weaker corotational flow that occurs without the cut off is associated with significantly increased pressure in the region near $\varphi = \varphi_{\rm p}$. This back pressure is affected by conditions a distance $\sim H$ from the planet and it can distort the streamline pattern close to the planet so that it becomes asymmetric as shown in Figs. 5 and 6. For the larger softening cases, the stagnation point is displaced azimuthally a distance $\sim br_{\rm p}$ from the location of the planet and the horseshoe width is reduced (see Fig. 3).

However, when the cut-off is applied, there is a single stagnation point at $\varphi = \varphi_{\rm p}$, slightly displaced from the radial location of the planet due to the radial pressure gradient of the unperturbed disc. The latter is a very minor effect that is absent from the local models on account of their strict symmetry. The local models always produce a single stagnation point at the location of the planet, a situation that is essentially recovered for small softening in simulations without a cut off (see also Fig. 3).

We take a closer look at this back pressure effect in Figs. 7 and 8, where we consider a slice through $r = r_{\rm stag}$, where $r_{\rm stag}$ is the radial location of the stagnation point. Because of the radial pressure gradient of the unperturbed disc, $r_{\rm stag} \neq r_{\rm p}$ (see Figs. 5 and 6). From equations (28) and (30) we know that the velocity is directly related to the gradient of χ. First of all, we can check if this approximation is valid. From the left panel of Fig. 7, we see that for both the full and the cut-off potential there is very good agreement between both v_x and v_y as measured from the simulation and the values expected from equations (28) and (30). Therefore, their assumption in the two dimensional model of section 3 should be a good approximation.

Note, however, the strong differences between the black

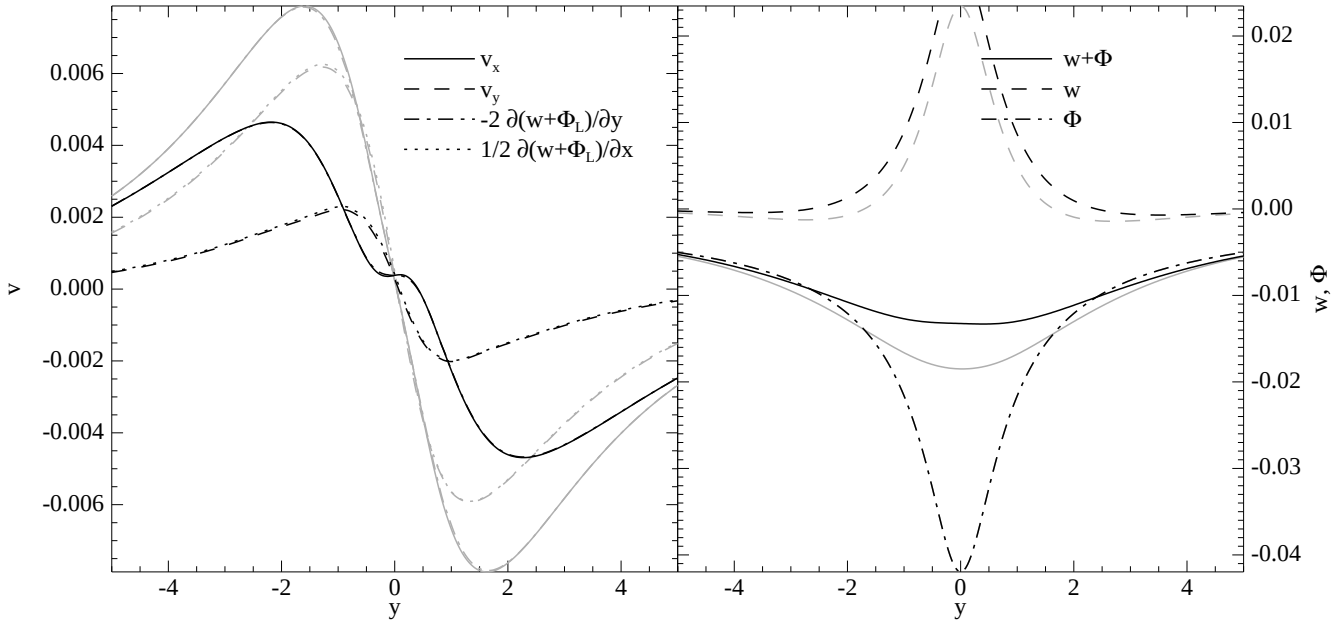

Figure 7. Velocities, enthalpy and planet potential at the radial location of the stagnation point for $q/h^3 = 0.0252$ and $b/h = 0.6$. Black curves indicate that the full planet potential was used, grey curves indicate results obtained with the cut-off procedure adopted.

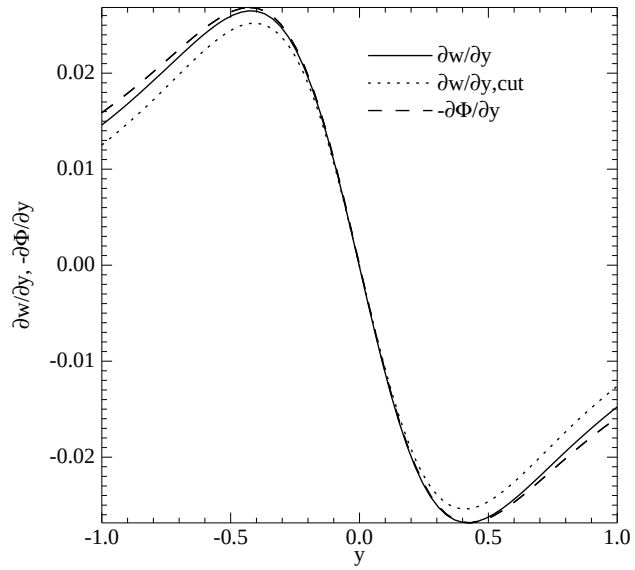

Figure 8. Derivatives of the enthalpy and the potential at the orbital radius of the stagnation point for $q/h^3 = 0.0252$ and $b/h = 0.6$.

curves for the full potential and the grey curves for the cut-off potential. Velocities are reduced due the back pressure originating at distances $\sim H$ from the planet when there is no cut off. The right panel of Fig. 7 clearly shows a higher peak in the enthalpy for the potential without a cut off. When added to the protoplanet potential the total is less in magnitude in that case and thus we can see from equations (28) and (30) that smaller inflow velocities will accordingly be produced.

The azimuthal shift of the stagnation point can be explained as follows. At a stagnation point, we must have that $\partial w/\partial y = -\partial\Phi_{\rm L}/\partial y$ (see equation (15)), since all velocities must vanish. When the cut-off is applied, there is only one stagnation point possible (see Fig. 8) at the azimuth of the planet. This is necessarily the case for a local model in the case of constant specific vorticity, because of symmetry arguments. Effects originating a distance $\sim H$ from the planet such as the production of the Lindblad wakes can destroy this symmetry by means of a back pressure effect. This increases the gradient of w near the planet, which, if strong enough, can give rise to three possible stagnation points. For the case shown in Fig. 8, the back pressure is such that one stagnation point appears, but shifted in azimuth by approximately one softening length. In Fig. 9, we show the y-derivative of $w + \Phi_{\rm L}$ at the radial location of the stagnation point.

When no cut off is used, the back pressure gives rise to a gradient of w at $y = 0$, pushing the stagnation point away from the planet. The actual configuration of the stagnation points depends on details in the flow, for example the background surface density gradient. Indeed, Masset et al. (2006) reported three stagnation points for the case with constant background surface density, a configuration that we find as well for the same surface density gradient. Since both the back pressure and the potential are proportional to q in the linear regime, the location of the stagnation points does not depend on the planet mass, which was also reported by Masset et al. (2006).

When $b \ll h$, the Lindblad torques will be largely independent of the softening parameter, since they are generated at distances much larger than $br_{\rm p}$ in this case. We then expect any related back pressure to be small, with any stagnation points located close to the planet. We find this indeed to be the case, and we see that for $b \ll h$ the agreement of $x_{\rm s}$ as measured from the simulations with that found using the model of Section 3, which does not take account

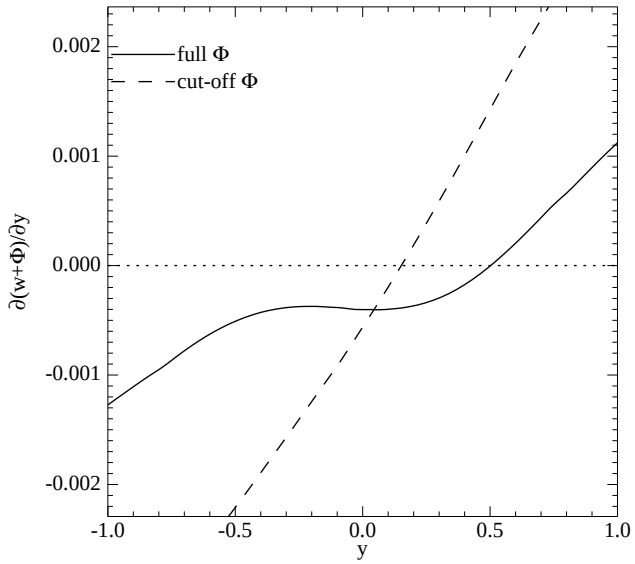

Figure 9. Derivative of the sum of the enthalpy and the potential at the orbital radius of the stagnation point for $q/h^3 = 0.0252$ and $b/h = 0.6$, with and without the cut off procedure.

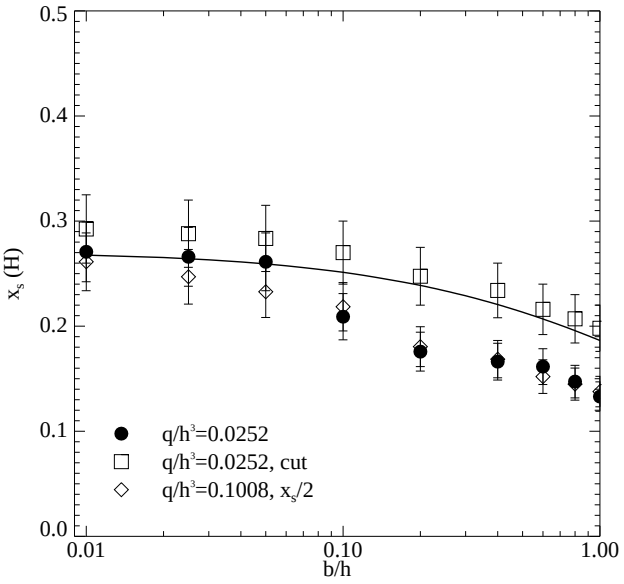

Figure 10. Half-width of the horseshoe region vs. softening parameter. Two planet masses are considered, the lowest one with and without the cut-off procedure. For the more massive planet $x_s/2$ is shown, to remove the $\sqrt{q}$ dependence. Error bars indicate an error of 10%.

of phenomena related to epicyclic motions such as Lindblad torques, is much better.

5.3 Width of the horseshoe region

We have measured the half-width of the horseshoe region x_s for various values of b and q though a streamline analysis. The results are shown in Fig. 10, with 10% error bars indicating our error estimate, for the cases with and without applying the cut off procedure. As indicated in our above discussion, horseshoe widths are always larger when the cut off procedure is applied. The deviation varying from about 10% at very small softening to 50% when $b \sim h$. The results predicted by the model in Section 4 with the two-dimensional Green's function are indicated by the solid curve. These are in good agreement with the other results for small softening but give values for $x_s \sim 20\%$ larger than those found from the simulations without a cut off procedure. It appears that these results fall below the others, because of the effect discussed above that we described as being due to a back pressure related to phenomena such as the wake produced at a distance $\sim 2H/3$ from the planet. As expected, for smaller values of b this effect is reduced.

In Fig. 10 we also show results for a planet with a mass that is four times larger (corresponding to 4 $M_\oplus$ orbiting a Solar mass star, embedded in a disc with $h = 0.05$). For this case, the measured value of x_s was divided by 2 to remove the $\sqrt{q}$ scaling. If $x_s \propto \sqrt{q}$ in this mass range, the black circles and diamonds should fall on top of each other in Fig. 10. It is clear that for all values of the softening parameter that we consider, the horseshoe width scales as $\sqrt{q}$ in this mass range. Masset et al. (2006) speculated that this scaling would brake down for softening parameters smaller than the Bondi radius. We find this not to be the case, since our smallest softening parameter $b < q/h^2$ for both planet masses placing it in that regime.

Although the perturbed surface density at the location of the planet can be quite large for small softening, this perturbation is almost in hydrostatic equilibrium and so does not play a major role in the flow, and does not cause a departure from $x_s \propto \sqrt{q}$. Below, we will argue that instead, while the value of b is important, this departure is governed by the ratio q/h^3.

Additional models with different values of H, while keeping b/h fixed, confirm that $x_s \propto 1/\sqrt{h}$ (see equation (39)) in the same mass range, as long as $x_s \ll H$.

5.4 Horseshoe drag

Ward (1991) found an expression for the corotation torque produced by material in the coorbital region in the form

$$\Gamma_{\rm c,hs} = \frac{3}{4}\left(\frac{3}{2}-\alpha\right) x_s^4 \Sigma r_p^4 \Omega_p^2, \tag{44}$$

where the surface density $\Sigma \propto r^{-\alpha}$, and all quantities are evaluated at $r = r_p$. On the other hand Tanaka et al. (2002) found an expression for the corotation torque derived from linear perturbation analysis in the form

$$\Gamma_{\rm c,lin} = 1.36\left(\frac{3}{2}-\alpha\right)\frac{q^2}{h^2}\Sigma r_p^4 \Omega_p^2. \tag{45}$$

Here we shall make use of these expressions, referring the reader to a companion paper for additional discussion.

We first note that although they are both torques, these expressions were derived for systems with differing flow topology and so should not be expected to be the same. The horseshoe drag applies to a system with the flow topology of our solutions for the coorbital region which has separatrices. On the other hand the linear corotation torque is derived from the linear perturbation theory of circular orbits.

The torque in both expressions is proportional to the vortensity gradient which cancels out when they are

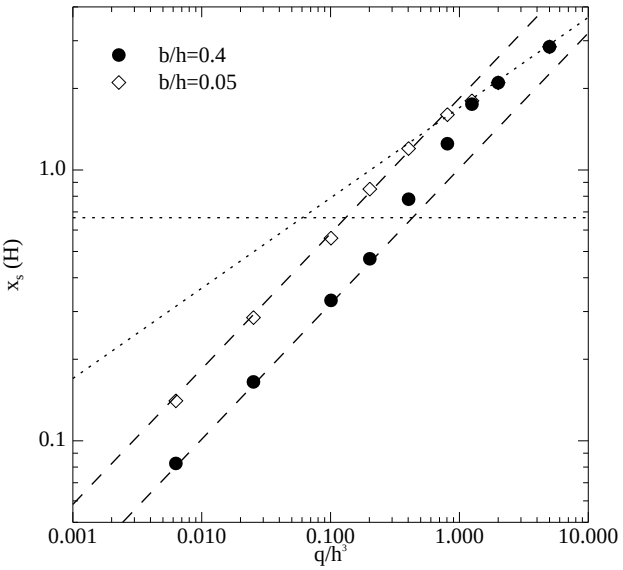

Figure 11. Half-width of the horseshoe region vs. mass ratio q, for two different values of b/h. The dashed lines indicate $x_\mathrm{s}|_{b=0}$, given by equation (40), and 0.6 times this value to account for the effects of softening and back pressure. The horizontal dotted line indicates $x_\mathrm{s} = 2H/3$. The tilted dotted line shows equation (47), expected to be valid at high masses.

equated. In this paper we considered only constant vortensity for which there is no torque. But we can consider the case of a small and smooth vortensity gradient, and following the discussion of section 3 we can argue, as has also been confirmed in simulations, that the horseshoe width should be close to that found assuming constant vortensity.

Masset et al. (2006) assumed that torques obtained from simulation results with $b/h = 0.3$ could be used to determine values of x_s by equating them to torques obtained from Tanaka et al. (2002) even though the latter were calculated for $b = 0$. The determined values of x_s agreed with those directly measured from the simulations, and we remark that our measurements of x_s for $b/h = 0.3$ agree with those of Masset et al. (2006).

However, from Fig. 10, we see that x_s increases by a factor of 1.67 as b decreases from $0.3h$ to zero. Therefore, the horseshoe drag torque, being proportional to x_s^4, is actually nearly an order of magnitude larger than the linear corotation torque for $b = 0$ and so *should not* be equated to it. It thus turns out that the combined effects of finite softening and the back pressure phenomenon discussed above reduced the estimated horseshoe drag by almost an order of magnitude compared to the value that should have been adopted to compare with Tanaka et al. (2002).

5.5 Extension to higher masses

When q/h^3 is of order unity, the Hill sphere, the Bondi radius and the half-width of the horseshoe region are all comparable to H. At approximately this mass, the waves excited by the planet start to become non-linear at a distance $\sim H$ from it, and gap formation sets in. This reduces the strength of the Lindblad torques and any influence of material at a distance $\sim H$, and therefore the back pressure effect described above. At the same time, the width of the horseshoe region, being proportional to $\sqrt{q/h}$, also becomes comparable to H, extending into the Lindblad resonance region. This also reduces the back pressure effect, making the horseshoe width larger. This was checked by running an additional model with $q/h^3 = 0.4032$ (8 $\mathrm{M}_\oplus$ embedded in a disc with $h = 0.05$ around a Solar mass star), $b/h = 1$ and $b/h = 0.2$. For $b/h = 1$, we find a horseshoe width of $x_\mathrm{s} = 0.54H$, which corresponds to an exact scaling $x_\mathrm{s} \propto \sqrt{q}$ according to Fig. 10. This is to be expected, since $x_\mathrm{s} < 2H/3$, and the horseshoe region does not extend into the wave excitation zone. For $b/h = 0.2$,, we find $x_\mathrm{s} = 0.9H$, while a scaling with $\sqrt{q}$ would imply $x_\mathrm{s} = 0.75H$, according to Fig. 10. Therefore, the horseshoe width is larger than predicted by the simple model, in agreement with the findings of Masset et al. (2006). We stress that this behaviour should not be seen as an onset of nonlinearity, since there is *no* horseshoe region in linear theory, but rather as a reduction of the back pressure effect of material at a distance $\sim 2H/3$ from the planet where the main Lindblad torques are produced on the horseshoe region.

The exact mass at which $x_\mathrm{s} = 2H/3$ of course depends on softening. If we write $x_\mathrm{s} = C(b)x_\mathrm{s}(b = 0)$, with $C(b) < 1$ and for an approximate estimate, set $x_\mathrm{s}(b = 0)/r_\mathrm{p} = 1.68\sqrt{q/h}$ (see equation (40)), we get:

$$q < q_\mathrm{trans} \equiv \frac{0.157h^3}{C(b)^2} \tag{46}$$

as a condition for $x_\mathrm{s} \propto \sqrt{q}$. For $b/h = 0.3$, as used by Masset et al. (2006), we have $C \approx 0.6$ (see Fig. 10), and therefore $q_\mathrm{trans} = 5.5 \cdot 10^{-5}$ for $h = 0.05$, exactly the mass at which the departure from linearity as reported by Masset et al. (2006) begins. Note that for the same parameters, the ratio of the Bondi radius to the softening parameter is approximately unity. However, for $C = 1$, we have $q_\mathrm{trans}/h^3 = 0.157$, confirming that for $q/h^3 = 0.1008$ and $q/h^3 = 0.0252$, as shown in Fig. 10, $x_\mathrm{s} \propto \sqrt{q}$ for all softening parameters, independent of the ratio of the Bondi radius to the softening. On the other hand, for $b \gg h$, using equation (41), it can be shown that $q_\mathrm{trans}/h^2 \propto b$. In this case, the critical value of b for which $q = q_\mathrm{trans}$ is proportional to the Bondi radius. However, such a large softening is incompatible with the idea of vertical averaging, from which we expect b to be of the order of h.

These ideas are further illustrated in Fig. 11, where we show the measured half-width of the horseshoe region versus planetary mass. For $q \ll h^3$, we expect $x_\mathrm{s} \propto \sqrt{q}$, with a coefficient that depends on the softening. For small softening, we see that the results agree very well with equation (40), while for large softening we find values that are a factor of 0.6 smaller due to the combined effect of non-zero softening and back pressure (see above). At higher masses, we expect x_s to be proportional to the radius of the Hill sphere (Pepliński 2008):

$$x_\mathrm{s} = 2.47 \left(\frac{q}{3}\right)^{1/3}, \tag{47}$$

indicated by the tilted dotted line in Fig. 11. For $q \gg h^3$ we find this indeed to be the case, independent of the value of b/h. The results for $b/h = 0.4$ are in very good agreement with Masset et al. (2006), who used $b/h = 0.3$, for all values of q. In between the two regimes of $x_\mathrm{s} \propto \sqrt{q}$ and $x_\mathrm{s} \propto q^{1/3}$

the width of the horseshoe region rises faster than $\sqrt{q}$, which is due to a reduction in the strength of the back pressure, as argued above. For $b/h = 0.05$, no such behaviour is found, since the effects of the back pressure are small for all q.

We therefore conclude that for $q > q_{\rm trans}$, the back pressure effect of the Lindblad torques is reduced, which leads to an increase in the width of the horseshoe region towards the value obtained from equation (39). This is consistent with the streamline analysis presented in Masset et al. (2006), where it is shown that in this transition regime only one stagnation point survives and moves towards the location of the planet. We have confirmed this behaviour in our simulations. This increase in $x_{\rm s}$ can have a major impact on the torque acting on the planet (see equation (44)).

6 DISCUSSION AND CONCLUSIONS

In this paper we presented a simple model of the coorbital region around a low mass planet. Using this we derived the horseshoe width as a function of planet mass and gravitational softening parameter. In the limit of zero softening we found that

$$\frac{x_{\rm s}}{r_{\rm p}} = 1.68\sqrt{\frac{q}{h}}. \tag{48}$$

This result agreed with high resolution numerical simulations to within several percent. However for softening lengths $br_{\rm p} \sim H$, the discrepancy was larger, with the simulations indicating a horseshoe width about 22% smaller. By considering simulations for which a cut off procedure was used to remove the effects of the protoplanet potential produced at and beyond a radial separation of $2/3H$ from it, it was found that phenomena at that separation could significantly affect the horseshoe width, even when that was much narrower, distorting the streamlines and reducing the width through the action of an additional back pressure that is more effective for larger softening. This may artificially reduce the horseshoe drag in such cases.

We also used our results to show that the horseshoe drag, exerted by material executing horseshoe turns is about an order of magnitude larger than the linear corotation torque in the zero softening limit. A more complete comparison between linear corotation torques and horseshoe drag for finite b requires additional linear calculations which are presented in detail in an accompanying paper. There we also find that the non-linear corotation torque (horseshoe drag) is always much larger than the linear corotation torque for non zero b.

We have focused on a two-dimensional description of the horseshoe region, with a softening parameter b in the planet potential which may approximately account for three-dimensional effects. As reported in Masset et al. (2006), the horseshoe drag torque appears to be stronger in fully three-dimensional simulations compared to two-dimensional runs that include softening. Clearly, a three-dimensional model of the horseshoe region is desirable. This will be the subject of a future investigation.

Another useful extension of the present discussion would be the inclusion of non-barotropic effects. We remark that the model presented in this paper is valid for discs that have a constant specific vorticity and entropy, the latter condition leading to a barotropic equation of state. Introducing a radial vortensity gradient breaks the up-down symmetry in Figs. 1-3, but simulations show that this effect is barely detectable. Thus we may expect that the prediction of the horseshoe width obtained from our simple model may work reasonably for non-barotropic discs with a radial entropy gradient. However, we do expect some difference in $x_{\rm s}$ between isothermal and non-isothermal discs. It is easy to see that $x_{\rm s}$, as obtained from equation (36), is proportional to $c_{\rm s}^{-1/2}$. For equal temperatures, the sound speed in an adiabatic disc is a factor $\sqrt{\gamma}$ larger than the isothermal sound speed, where γ is the adiabatic exponent. This makes the horseshoe region a factor $\gamma^{1/4}$ smaller in adiabatic simulations. Although the difference lies within our 10% error bars, we have noticed it when comparing our present results with those in Paardekooper & Papaloizou (2008). Note that this makes the adiabatic horseshoe drag, being proportional to $x_{\rm s}^4$, a factor γ smaller than the isothermal horseshoe drag. Since also the wave torque scales as γ^{-1}, the relative strength of the Lindblad torques and horseshoe drag remains the same for adiabatic discs.

The shape of the horseshoe region changes when a global radial mass flow is introduced with respect to the planet. This mass flow can be due to viscous accretion, but also due to radial movement of the planet when allowing the orbit of the planet to change. When the time scale of the radial flow with respect to the planet to cross the horseshoe region is smaller than the libration time scale, an asymmetry between the sides of the horseshoe region leading and trailing the planet develops (Artymowicz 2004). This is important for studying Type III migration (Masset & Papaloizou 2003). In this paper, we have kept the planet on a fixed orbit in an inviscid disc, and therefore such effects did not occur. More work is necessary to study the importance of including the effect of planetary migration on the disc response and torques for low-mass planets.

ACKNOWLEDGEMENTS

We thank the anonymous referee for an insightful report. This work was performed using the Darwin Supercomputer of the University of Cambridge High Performance Computing Service (http://www.hpc.cam.ac.uk), provided by Dell Inc. using Strategic Research Infrastructure Funding from the Higher Education Funding Council for England.

REFERENCES

Artymowicz P., 2004, in Caroff L., Moon L. J., Backman D., Praton E., eds, ASP Conf. Ser. 324: Debris Disks and the Formation of Planets Dynamics of Gaseous Disks with Planets. p. 39
Baruteau C., Masset F., 2008, ApJ, 672, 1054
Crida A., Morbidelli A., 2007, MNRAS, 377, 1324
D'Angelo G., Henning T., Kley W., 2002, A&A, 385, 647
D'Angelo G., Kley W., Henning T., 2003, ApJ, 586, 540
Goldreich P., Tremaine S., 1979, ApJ, 233, 857
Goldreich P., Tremaine S., 1980, ApJ, 241, 425
Korycansky D. G., Papaloizou J. C. B., 1996, ApJS, 105, 181
Korycansky D. G., Pollack J. B., 1993, Icarus, 102, 150

Lin D. N. C., Papaloizou J., 1986, ApJ, 309, 846
Masset F. S., D'Angelo G., Kley W., 2006, ApJ, 652, 730
Masset F. S., Papaloizou J. C. B., 2003, ApJ, 588, 494
Mayor M., Queloz D., 1995, Nature, 378, 355
Nelson R. P., Papaloizou J. C. B., 2004, MNRAS, 350, 849
Ogilvie G. I., Lubow S. H., 2002, MNRAS, 330, 950
Paardekooper S.-J., Mellema G., 2006a, A&A, 459, L17
Paardekooper S.-J., Mellema G., 2006b, A&A, 450, 1203
Paardekooper S.-J., Mellema G., 2008, A&A, 478, 245
Paardekooper S.-J., Papaloizou J. C. B., 2008, A&A, 485, 877
Papaloizou J. C. B., Nelson R. P., Kley W., Masset F. S., Artymowicz P., 2007, in Protostars and Planets V Disk-Planet Interactions During Planet Formation. pp 655–688
Pepliński A., 2008, PhD thesis, Department of Astronomy, Stockholm University, Stockholm, Sweden
Pepliński A., Artymowicz P., Mellema G., 2008a, MNRAS, 386, 179
Pepliński A., Artymowicz P., Mellema G., 2008b, MNRAS, 387, 1063
Tanaka H., Takeuchi T., Ward W. R., 2002, ApJ, 565, 1257
Ward W. R., 1991, in Lunar and Planetary Institute Conference Abstracts Horsehoe Orbit Drag. p. 1463
Ward W. R., 1997, Icarus, 126, 261